Chapter 5

Ionic Liquid-Induced Unique Structural Transitions of Proteins

Takahiro Takekiyo and Yukihiro Yoshimura

Additional information is available at the end of the chapter

http://dx.doi.org/10.5772/65886

Abstract

The structural transitions of proteins in aqueous solutions of various ionic liquids (ILs) over a wide concentration range (x (mol% IL) = 0–30) were investigated using Fourier-transform infrared and near-UV circular dichroism spectroscopy combined with small-angle X-ray scattering. The proteins in the aqueous IL solutions showed two structural transition patterns: (i) the folded state → unfolded state → partial globular state (α-helical formation disrupted tertiary structure) and (ii) the folded state → unfolded state → aggregation (amyloid-like aggregation or disordered aggregation). We found that the helical formation of proteins in the condensed IL solutions was strongly related to the competition between the low polarity and denaturation effect of ions. Moreover, the amyloid-like aggregate formation correlated with the competition between the size of the confined water assemblies in the IL layer and the IL-amino acid residue interactions. On the basis of these results, we discussed the future applications of ILs, including their use as cryoprotectants for proteins and as agents for the suppression of amyloid formation.

Keywords: protein, aqueous ionic liquid solution, aggregation, helix formation, optical spectroscopy

1. Introduction

Aqueous mixtures of proteins and ionic liquids (ILs), which comprise organic cations and anions and remain in the liquid state below 373 K, are employed in protein engineering applications, such as protein storage media, biocatalysts, and buffers [1–3]. Although these applications are based on the unique solvent properties of these mixtures, such as their solubility in water and solution structure [2, 4], the detailed relationship between the proteins and aqueous IL solutions at the molecular level is unclear. Thus, to realize the protein engineering

applications of ILs, numerous studies have been conducted on the structural stability and activity of proteins in aqueous IL solutions [2–8].

For instance, Lange et al. [6] demonstrated that the addition of imidazolium-based ILs (up to 4 M) to renaturation buffers caused high protein renaturation without protein aggregation, whereas addition to the folded protein induced a decrease in the structural stability. Many aqueous IL solutions are found to degrade the structural stability and activity of proteins at x (mol% IL) < 6 [2, 3, 7, 8]. This decrease in protein stability in dilute aqueous IL solutions can be explained by the Hofmeister series [7, 8]. This series ranks the relative influence of ions on the physical behavior of a wide variety of aqueous processes ranging from colloidal assembly to protein folding. Originally, it was assumed that the influence of ions on protein folding was caused at least in part by "making" and "breaking" bulk water structures [9]. However, these investigations of protein stability in dilute aqueous IL solutions have not sufficiently considered essential properties of ILs. Thus, it is necessary to obtain basic information on protein stability over a wide IL concentration range to realize protein engineering using ILs.

Recently, intriguing phenomena such as protein refolding and aggregate formation have been observed in condensed IL solutions ($x > 10$) or pure IL. Imidazolium-based or alkylammonium-based ILs at a concentration of $x > 10$ induce the formation of α-helical structures of protein, such as human interleukin-2 [10] and succinylated concanavalin A [11]. Moreover, Hwang et al. [12] showed that imidazolium- and pyridinium-based ILs promoted amyloid formation in α-synuclein and α-lactalbumin. Similarly, Debeljuh et al. [13] demonstrated that addition of protic ILs, such as triethylammonium-based ILs, to Aβ1–40 peptide promotes amyloid aggregation. These intriguing protein-refolding/amyloid-formation phenomena in condensed ILs or pure ILs may be related to the essential properties of ILs and cannot be explained by Hofmeiester series, as in the case of protein unfolding in dilute aqueous IL solutions.

Related to these phenomena, the solvent properties of ILs, such as viscosity and dielectric constant, drastically change at a certain IL concentration [2]. These changes depend on the amount of water in the mixture. In addition, it is known that IL solutions adopt a nanoheterogeneous structure with a polar domain, i.e., the ionic parts of the cations and anions, and a nonpolar domain, i.e., the alkyl chain of the cations [14–16]. In binary solutions under water-rich conditions [17], IL-water mixtures adopt IL-aggregated structures that are surrounded by bulk water molecules; therefore, the nanoheterogeneity of these systems is relatively low. However, under IL-rich conditions wherein the mixtures exhibit molten-salt-like behavior, the water molecules are scattered in the polar domain and self-assemble in the ILs. The water molecules in this state are termed "confined water" [18, 19] and the nanoheterogeneity of these systems is higher. As mentioned earlier, these solvent properties may contribute to unique structural transitions of the proteins. Thus, detailed information on protein stability over a wide range of IL concentrations is valuable, and this information would facilitate the use of ILs in protein engineering applications.

This manuscript aims to determine the structural stabilities of various model proteins over a wide concentration range of ILs using optical spectroscopy combined with small-angle X-ray scattering (SAXS). The origin of the structural transitions of proteins in condensed aqueous IL solutions has been discussed.

2. Experimental methodology

2.1. Materials

Chicken lysozyme, bovine ribonuclease A (RNase A) and bovine β-lactoglobulin (β-LG), horse cytochrome *c*, bovine myoglobin, bovine rhodanese, and bovine insulin were purchased from Sigma and were used without further purification. The ILs 1-butyl-3-methylimidazolium chloride ([bmim][Cl]) (Kanto Chemical Co.), [bmim][NO_3] (Sigma), [bmim][SCN] (Sigma), 1-ethyl-3-methylimidazolium nitrate ([emim][NO_3]) (Iolitec), methylammonium nitrate (MAN) (Iolitec), ethylammonium nitrate (EAN) (Iolitec), and propylammonium nitrate (PAN) (Iolitec) were used in this study. All aqueous mixtures with concentrations of x (mol% IL) were prepared by mixing the required amount of the IL and D_2O (Kanto Chemical Co.) at room temperature. The prepared concentrations of the aqueous IL solutions were x = 0–30 because of the overlap of the cations with proteins in the Fourier-transform infrared (FTIR) spectra. The concentrations of the proteins were adjusted to 20 mg mL^{-1}, which does not result in protein aggregation in water (x = 0). Samples were loaded into a transmission cell with CaF_2 windows and a Teflon spacer (50 μm) for FTIR and near-UV circular dichroism (CD) spectral measurement under the same protein conditions as used in the condensed ILs. These spectral analyses were performed using the GRAMS software (Galactic Software).

2.2. FTIR spectroscopy

The amide I′ vibrational mode (deuterated peptide groups) in FTIR spectra is highly sensitive to the secondary structure of proteins, and thus it serves as an indicator of α-helix and β-sheet formation [20]. FTIR spectra were recorded using a Nicolet 6700 FTIR spectrometer equipped with a mercury-cadmium-telluride liquid-nitrogen detector. Typically, 512 interferograms were collected to obtain spectra with a resolution of 4 cm^{-1}. Solvent spectra were also measured under the same conditions as those used for the protein solution measurements and were subtracted from the protein solution spectra.

2.3. CD spectroscopy

Near-UV CD spectra in the range of 250–300 nm are sensitive to the presence of specific rigid packing interactions between aromatic side chains, indicating changes in the tertiary structure [21]. CD spectra were measured over a wavelength range of 250–300 nm on a JASCO J-820 spectropolarimeter. Typically, spectra were accumulated at a scan rate of 20 nm min^{-1} in 0.1 nm steps. Five scans were averaged for each spectrum. The obtained spectra were converted into mean residue ellipticity units using $[\theta] = \theta_{obs}/(10ncl)$, where θ_{obs} is the observed ellipticity, l is the path length, c is the protein concentration, and n is the number of residues.

2.4. SAXS

SAXS is a powerful technique for investigating protein size and the presence of protein aggregation [22]. SAXS experiments were conducted using a Kratky camera system (BioSAXS-1000, Rigaku Co.) at a brilliance of 56.0 kW mm^{-2}. CuKα radiation (λ = 0.1542 nm) was selected and

collimated using a parabolic multilayer mirror. The beam was focused by a converting optical tool (CBO-*f*, Rigaku Co.). The beam size was 0.5 mm (V) × 0.1 mm (H) at the sample position, and the camera distance was 500 mm. The combination of the 2D Kratky block and focusing optics can achieve a wide q range. Here the scattering vector q is defined as $4\pi\sin\theta/\lambda$ (nm^{-1}). A 2D detector (PILATUS 100 K/R) was used. Samples were put into quartz capillaries with a diameter of 1.0 mm and a thickness of 0.1 mm. The scattering of the aqueous IL solutions was subtracted, and the final scattering curve was obtained using the program *PRIMUS*.

3. Results and discussion

3.1. Structural transition of proteins in aqueous solutions with [bmim]-based ILs

As representative results, **Figure 1a** and **b** shows the FTIR amide I′ spectra of myoglobin and cytochrome *c* in aqueous solutions under concentrations of [bmim][NO_3] up to x = 30. The amide I′ spectra of both proteins change significantly as a function of [bmim][NO_3] concentration. The peaks at ca. 1615 and ca. 1690 cm^{-1}, which are due to the intermolecular β-sheet structure and indicate myoglobin aggregation [23], are observed above x = 5. However, no such peaks appear for cytochrome *c* over the studied [bmim][NO_3] concentrations.

To further investigate the changes in the secondary structure of both proteins, we plotted the changes in the maximum absorbance (Abs) values of these two proteins against the [bmim][NO_3] concentrations, as shown in **Figure 1c** and **d**. For myoglobin, the first decrease in the Abs value, indicating myoglobin unfolding, is observed in the region x = 1–5. The second decrease in the Abs value, indicating the formation of an intermolecular β-sheet structure, is observed at $x > 7$. Thus, the addition of [bmim][NO_3] to myoglobin causes the fold → unfold → intermolecular β-sheet transition.

Conversely, a drastic decrease in Abs for cytochrome *c* is observed up to $x = 7$, and it is noteworthy that the Abs value increases at $x > 7$. From the second-derivative analysis of the FTIR spectra, the peak at ca. 1645 cm^{-1} indicates an increase in the disordered structure up to x = 7, and further addition causes the increase in the peak at ca. 1655 cm^{-1}, which indicates an α-helical structure (inset in **Figure 1d**). Based on these FTIR spectra, the increase in Abs at $x > 7$ is due to the partial refolding of the secondary structure of cytochrome *c*. However, the partial refolding at $x > 7$ is not sufficiently confirmed by only the FTIR result. If the partial refolding of cytochrome *c* occurs at $x > 7$, the whole cytochrome *c* size would be smaller than in the unfolded state and larger than in the folded state. Therefore, to further investigate the state of cytochrome *c* in aqueous [bmim][NO_3] solutions, we performed SAXS measurements.

Figure 2a shows a Guinier plot of cytochrome *c* in aqueous [bmim][NO_3] solutions where the radius of gyration (R_g) was estimated. The Guinier equation is defined as follows:

$$I(q) = I(0)\exp(-R_g{}^2q^2) \tag{1}$$

where $I(0)$ is the intensity at $q = 0$. The Guinier equation is valid in the range of $R_gq < 1$. In this study, despite the fact that the range $0 < R_gq < 2$ was employed, a linear relationship in the

Guinier plots is observed. In aqueous [bmim][NO_3] solutions, the R_g values of cytochrome *c* were obtained in the same manner. The R_g values of cytochrome *c* are 13.4 Å for $x = 0$, 25.0 Å for $x = 5$, and 15.0 Å for $x = 20$. The R_g values at $x = 0$ and 5 are in good agreement with those of the folded state ($R_g = 13.8$ Å) and unfolded state ($R_g = 24.0$ Å) reported by Cinelli et al. [24]. As speculated above, the R_g value of cytochrome *c* at $x = 20$ is larger than that at $x = 0$ and smaller than that at $x = 5$. Thus, cytochrome *c* at $x = 20$ takes a more compact structure than at $x = 5$ and does not completely unfold without aggregation.

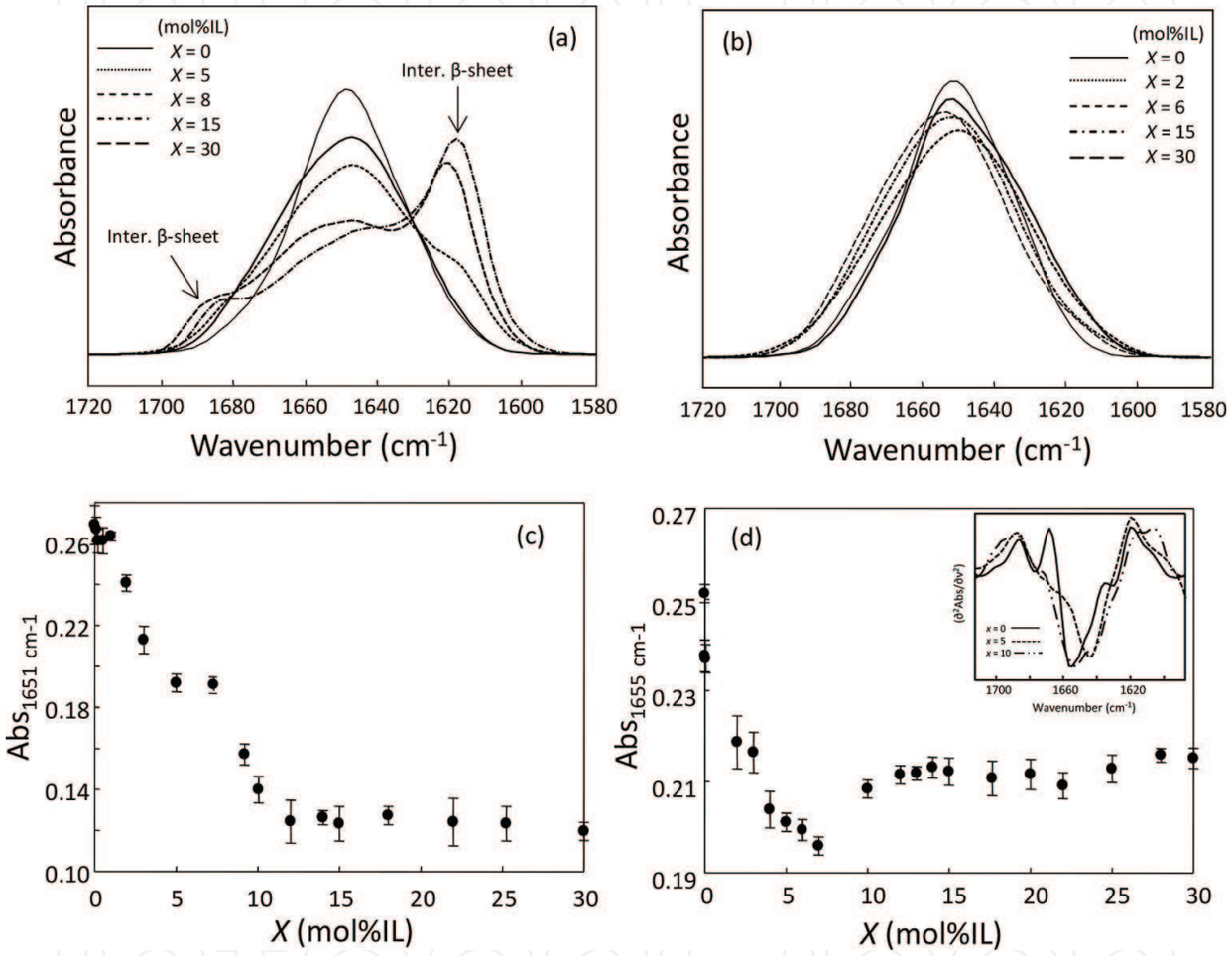

Figure 1. FTIR spectra in the amide I′ region of (a) myoglobin and (b) cytochrome *c* in aqueous [bmim][NO_3] solutions at several [bmim][NO_3] concentrations. Changes in absorbance of (c) myoglobin ($Abs_{1651cm-1}$) and (d) cytochrome *c* ($Abs_{1655cm-1}$) as a function of [bmim][NO_3] concentration. Inset figure shows the second derivative spectra of cytochrome *c* in aqueous [bmim][NO_3] solutions at $x = 0$, 5, and 10, respectively.

A similar result is also obtained using Kratky plots (**Figure 2b**). Kratky plots provide insight into the compactness of a protein, i.e., a bell shape in the plot indicates a globular protein, whereas a plateau, seen in the high *q* region, suggests that the protein is unfolded. The addition of [bmim][NO_3] shifts the peak of the bell shape to a smaller *q* region, indicating that the size of cytochrome *c* increases with increasing [bmim][NO_3] concentration. This implies that cytochrome *c* in aqueous [bmim][NO_3] solutions, even at high [bmim][NO_3] concentrations, is not completely unfolded. Combination with FTIR and SAXS

results indicate that the aqueous [bmim][NO_3] solution at x = 20 causes cytochrome c to partially refold without aggregation.

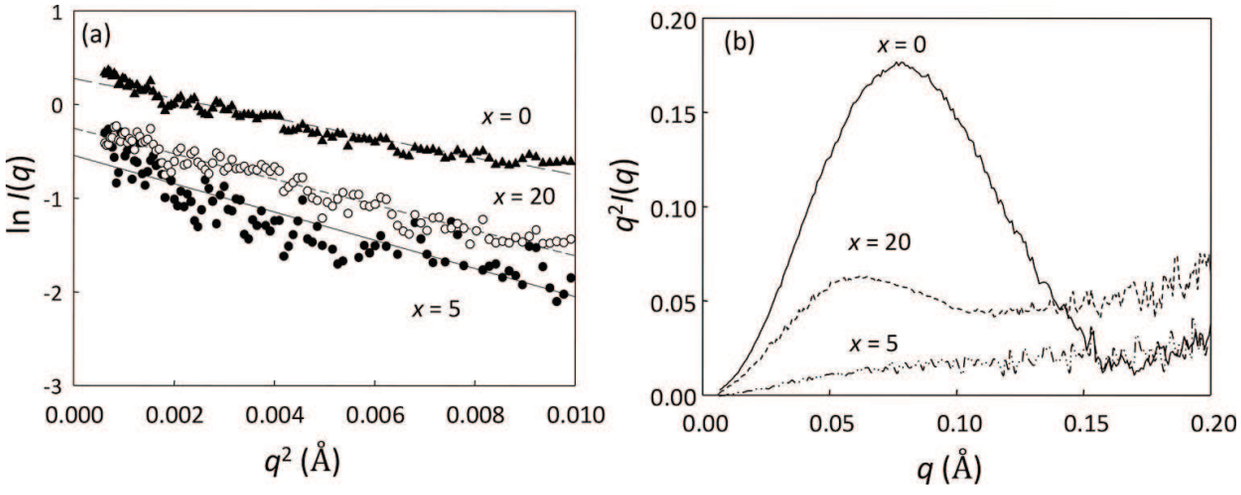

Figure 2. (a) Guinier plots and (b) Kratky plots of cytochrome c in aqueous [bmim][NO_3] solutions at x = 0, 5, and 20.

Next, we measured the changes in the tertiary structure of both proteins induced by [bmim][NO_3] using near-UV CD spectroscopy (**Figure 3a** and **b**). Although the negative CD intensity at 290 nm for myoglobin and 288 nm for cytochrome c due to the aromatic residues drastically decreases at [bmim][NO_3] concentrations of up to x = 7, no increase in the negative CD intensity occurs above x = 7 (**Figure 3c** and **d**). This indicates that an increase in the [bmim][NO_3] concentration completely disrupts the tertiary structure of both proteins.

The results from the FTIR, SAXS, and near-UV CD analyses show that aqueous [bmim][NO_3] solutions of up to x = 5–7 cause myoglobin and cytochrome c to unfold. Further addition of [bmim][NO_3] induces formation of the intermolecular β-sheet for myoglobin and the partially globular (PG) state, which is the α-helical formation disrupted tertiary structure, for cytochrome c. Consequently, changes in the concentration of [bmim][NO_3] induce structural transitions of the folded state → unfolded state → intermolecular β-sheet aggregation for myoglobin, and the folded state → unfolded state → PG state for cytochrome c. Similar structural transitions are observed in other proteins (β-LG, lysozyme, and RNase A) in aqueous solutions with other [bmim]-based ILs ([bmim][Cl] and [bmim][SCN]), except for cytochrome c in condensed [bmim][SCN] solutions (cytochrome c in this media takes the disordered-rich aggregate) [24–28]. **Figure 4** summarizes the structural transitions of proteins in aqueous solutions over a wide IL concentration range.

The most remarkable result is that condensed solutions with [bmim]-based ILs cause the formation of an α-helical structure, and intermolecular β-sheets or disordered-rich aggregation. From the previous results, the former state is similar to the intermediate in the on- or off-pathway for the protein folding process [29], and the latter state is similar to the amyloid structure associated with neurodegenerative conditions such as Parkinson's disease [30, 31] and the structure of the inclusion body in expression proteins [30, 32]. Thus, it is important to reveal the origin of the structural formation of proteins in condensed aqueous IL solutions in

http://dx.doi.org/10.5772/65886

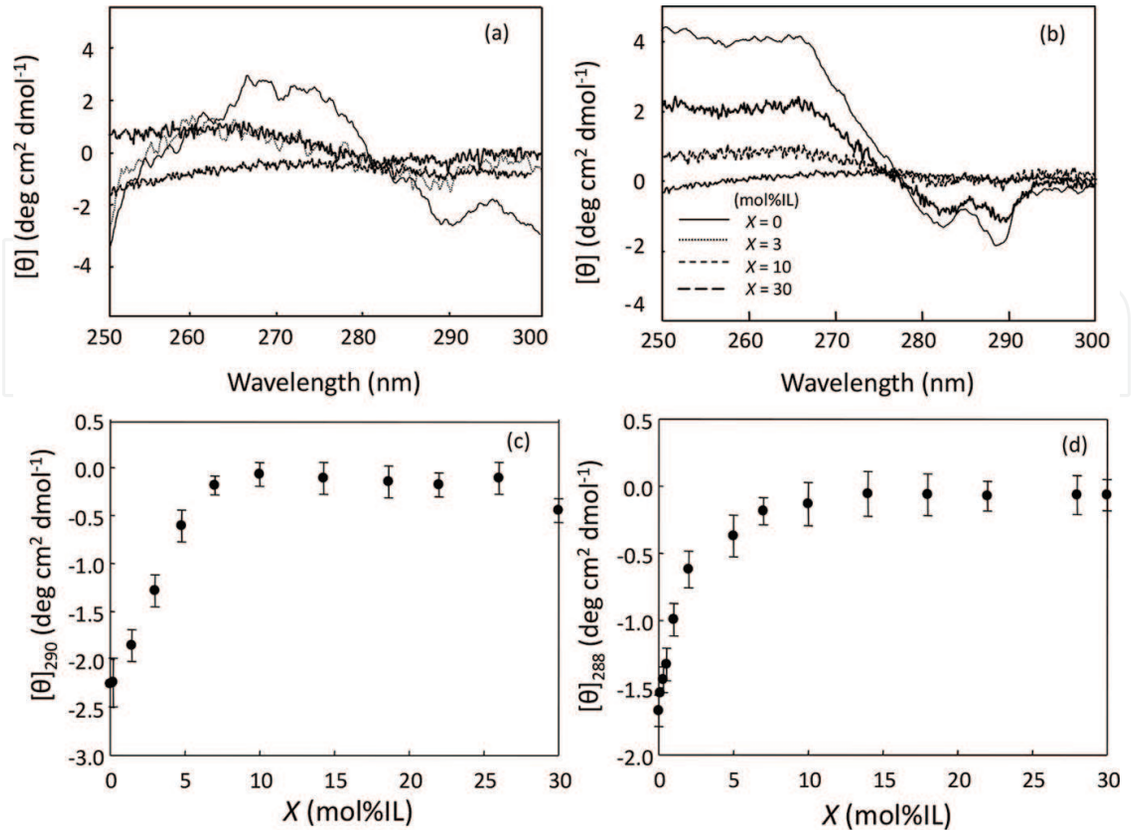

Figure 3. Near-UV CD spectra in the amide I′ region of (a) myoglobin and (b) cytochrome *c* in aqueous [bmim][NO_3] solutions at several [bmim][NO_3] concentrations. Changes in ellipticity of (c) myoglobin ($[\theta]_{290}$) and (d) cytochrome *c* ($[\theta]_{288}$) as a function of [bmim][NO_3] concentration.

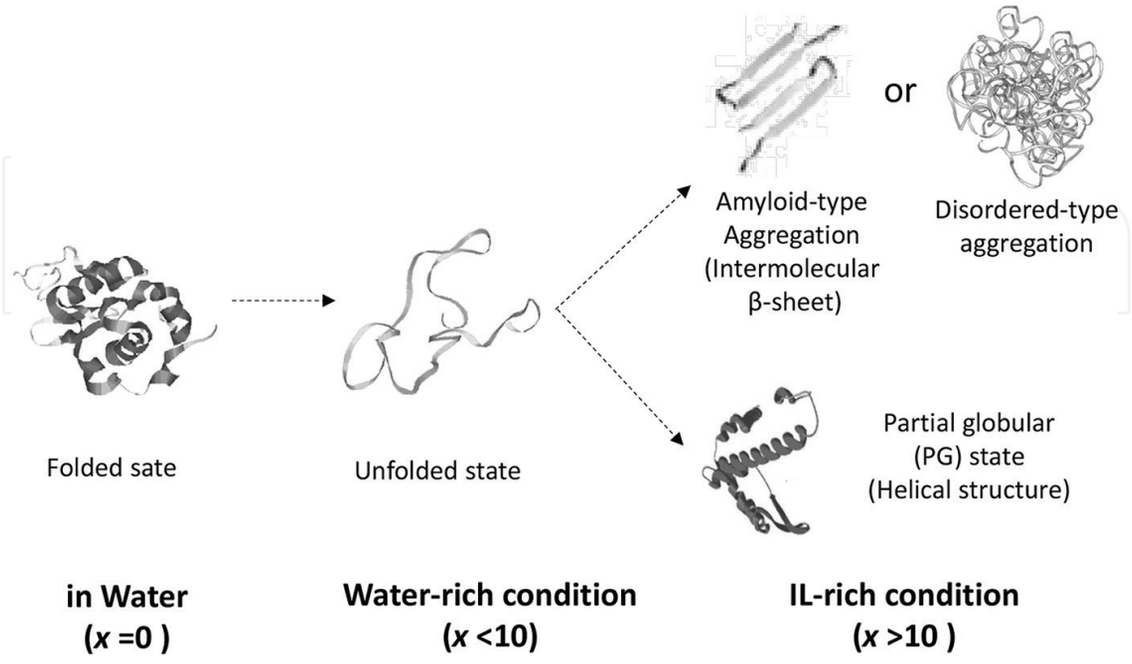

Figure 4. Summary of structural transition of proteins in aqueous ILs solutions.

view of protein engineering application using ILs. In the following sections, we discuss the preferential formation of the α-helical structure (PG state) in Section 3.2, and intermolecular β-sheet aggregation in Section 3.3.

3.2. Helix formation ability of ILs for proteins

We found that condensed aqueous solutions with [bmim]-based ILs induce the helical formation disrupted tertiary structure (PG state) for some proteins. Generally, it is well known that β-LG and RNase A, having substantial β-sheet contents, take non-native helical formations in aqueous alcohol solutions, such as 2,2,2-trifluoroetahnol [33–35]. This is termed alcohol denaturation. The PG state in condensed IL solutions structurally resembles that from alcohol denaturation. Here, we focused on the details of helical formation ability of ILs for β-LG and RNase A.

Figure 5a and **b** shows the FTIR spectra of β-LG and RNase A in aqueous [bmim][NO_3] solutions of several concentrations. On the whole, the absorbance of both proteins at ca. 1635 cm^{-1}, indicating intramolecular β-sheet structure, decreases, and that at ca. 1656 cm^{-1}, indicating the α-helix structure, increases with [bmim][NO_3] concentration (**Figure 5a** and **c**). Both proteins undergo helix formation at high [bmim][NO_3] concentrations, though β-LG forms an intermolecular β-sheet structure in addition to an α-helical structure. Characterization of the helix formation in condensed aqueous [bmim][NO_3] solutions reveals that it is similar to that seen for alcohol denaturation, which results in a direct β-α transition. However, it is intriguing whether the condensed [bmim][NO_3] solutions induce direct β-α transition, as in the case of alcohol denaturation.

We assessed the second-derivative FTIR spectra of β-LG and RNase A in aqueous [bmim][NO_3] solutions at different concentrations of [bmim][NO_3] (**Figure 5c** and **d**). Increasing the [bmim][NO_3] concentration up to x = 1–5 causes a decrease in the intramolecular β-sheet structure and an increase in the disordered structure of both proteins. With further addition of [bmim][NO_3] (up to x = 30), the disordered structure decreases and the α-helical content increases. Conversely, our previous FTIR spectra showed that the intramolecular β-sheet structure of β-LG in the aqueous TFE solution drastically decreases with increasing TFE concentration, and the α-helical content increases without the appearance of the disordered structure [26]. Importantly, the metastable intermediate, i.e., native β-sheet → disordered structure → non-native α-helix, in the β-α transition process, can be observed in aqueous [bmim][NO_3] solutions. Unlike alcohol denaturation (direct β-α transition), the aqueous [bmim][NO_3] solutions cause helix formation in β-LG and RNase A through an intermediate disordered structure. Although similar helix formation ability is observed in [bmim][Cl], its ability is weaker than [bmim][NO_3]. Besides, [bmim][SCN], representing a strong denaturant, does not show helix formation ability.

Here we discuss the origin of helix-forming ability of [bmim]-based ILs for β-LG and RNase A. Generally, alcohol denaturation is thought to arise from solvent properties such as low polarity. Low solvent polarity weakens the hydrophobic interactions that stabilize the compact native structure of proteins while simultaneously strengthening the intramolecular electrostatic interactions, such as hydrogen bonds, and stabilizing secondary structures, particularly the α-helix. The dielectric constant (ε) of the [bmim]-based ILs is low (ε = 10–20) [36], similar

http://dx.doi.org/10.5772/65886

to that seen in alcohols (32.6 for methanol [37] and 27 for TFE [38]). The results suggest that [bmim]-based ILs cause an enhancement of the intramolecular hydrogen bonding in proteins by removing water molecules from their proximity. Accordingly, the similar solvent polarity of aqueous [bmim]-based ILs and aqueous alcohol solutions likely causes the structural changes observed for both proteins and stabilizes their α-helix structure. While the condensed [bmim][SCN] solutions, which is a strong denaturant, did not show the helix formation for β-LG and RNase A. Thus, the helix-forming ability of [bmim]-based ILs depended on the anionic species, and is related to the competition between the low polarity of condensed IL and denaturant effect of anions showing the anion-protein interaction.

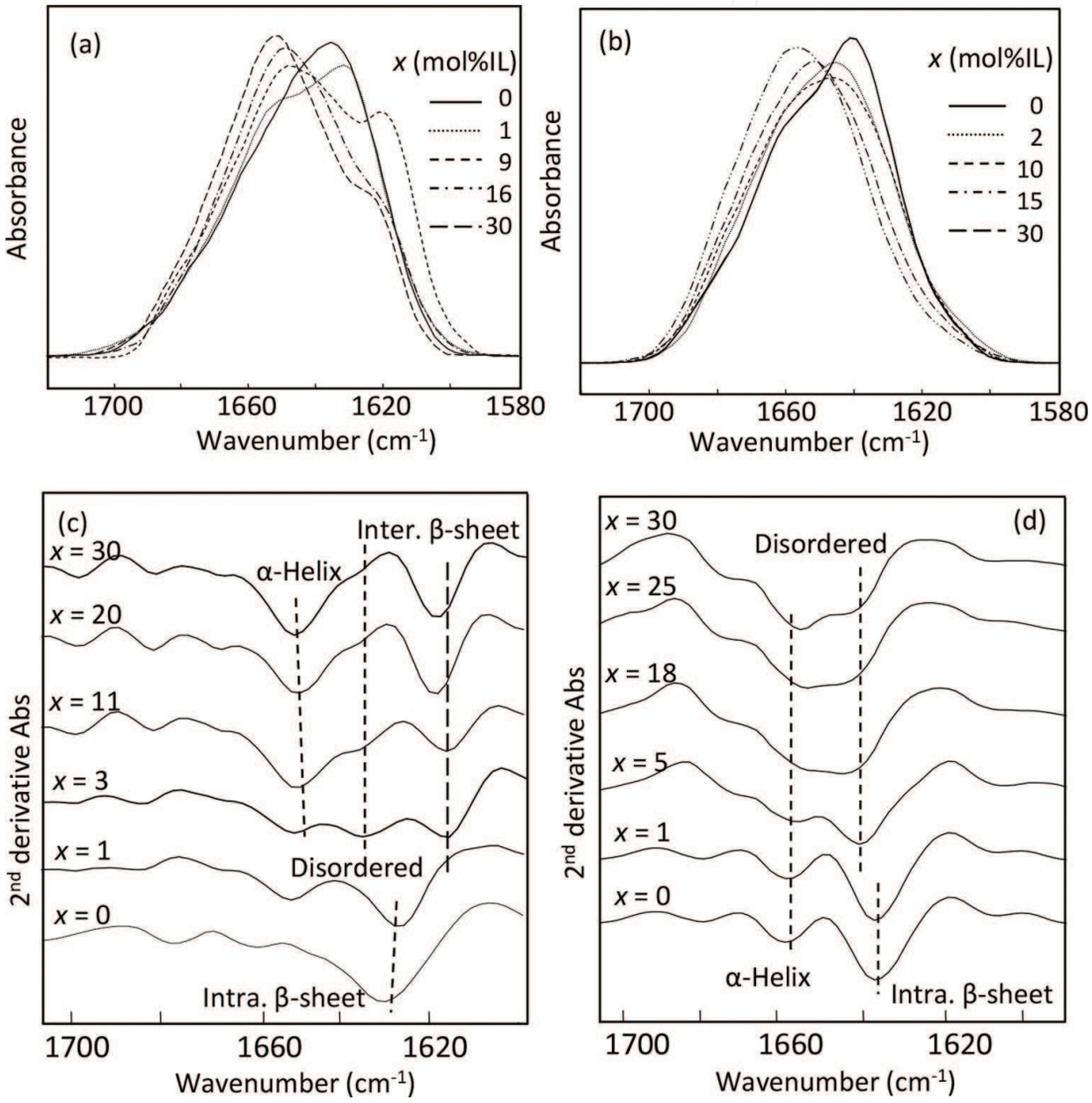

Figure 5. FTIR (a and b) and second derivative (c and d) spectra of β-LG and RNase A in aqueous [bmim][NO_3] solutions at several [bmim][NO_3] concentrations.

Next we discuss the generality of helix formation of ILs with NO_3^-. The helix-forming ability of [bmim][NO_3] for proteins has been connected to its low polarity; however, similar solution properties are also observed in other ILs with NO_3^-anion. To elucidate the generality of helix formation of β-sheet-rich proteins in ILs with NO_3^-, we compared two imidazolium-based ILs ([bmim][NO_3] and 1-ethyl-3-methylimidazolium nitrate ([emim][NO_3])) and the three alkylammonium nitrates (RAN-ILs): MAN, EAN, and PAN.

As a representative result, the FTIR spectra of RNase A in condensed aqueous solutions with various ILs at x = 30 are shown in **Figure 6a**. Although the FTIR spectral shape of RNase A in MAN shows slight RNase A unfolding, those with other ILs show a decrease in the native sheet structure and an increase in the helix structure. The amounts of α-helix structures in RNase A and β-LG were determined using a curve-fitting method (**Figure 6b**). Notably, the amounts of α-helix structures in RNase A (○) and β-LG (●) with the ILs (except for MAN) are essentially the same (within estimated experimental errors). This indicates that the effect of IL cations on the secondary structure of both proteins is negligible. The orders of solvent-induced helix formation of RNase A and β-LG are D_2O << MAN << [emim][NO_3] < EAN ~ PAN ~ [bmim][NO_3] (the value of α-helical content of β-LG in [bmim][NO_3] is slightly lower than those in EAN, PAN, and [bmim][NO_3] by the formation of intermolecular β-sheets). The present results indicate that condensed aqueous ILs with NO_3^- solutions show a high helix-forming ability for β-sheet-rich proteins, such as RNase A and β-LG.

On the basis of these results, we can conclude that the helix-forming ability of IL depended on the anionic species rather than the cationic species. Besides, this ability is strongly related to the competition between the low polarity and denaturation effect of anions.

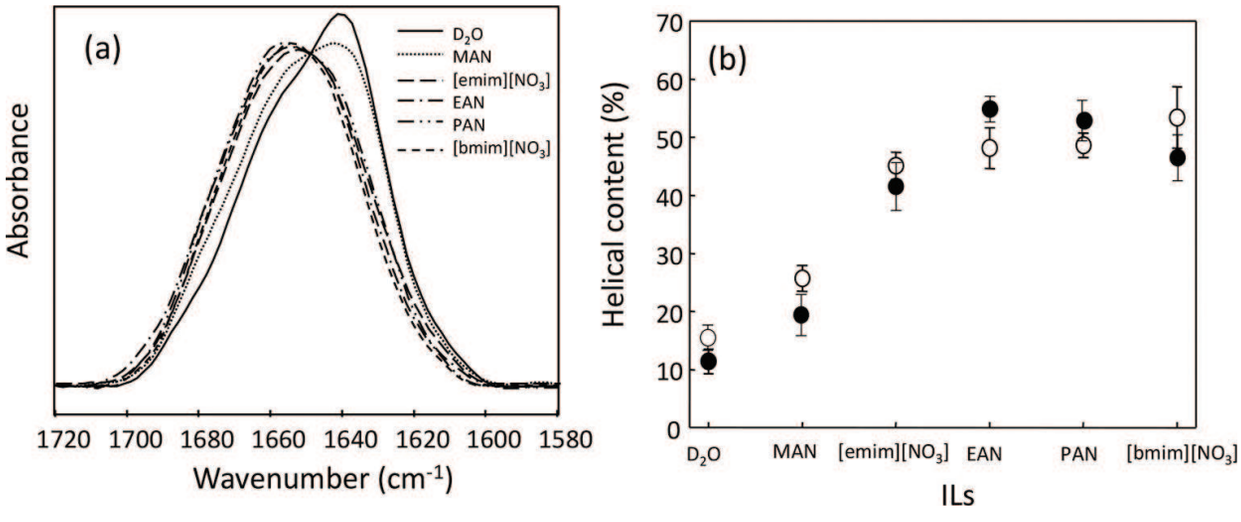

Figure 6. (a) FTIR spectra in the amide I′ region of RNase A at various ILs with NO_3^- (x = 30). (b) Contents of the α-helical structures of RNase A and β-LG at various ILs with NO_3^- (x = 30).

3.3. Ionic liquid-induced amyloid-like aggregation

Another intriguing phenomena associated with condensed IL solutions are the formation of intermolecular β-sheet structures (i.e., amyloid-like aggregation). As mentioned in Section 3.1,

amyloid-like aggregation is related to neurodegenerative diseases such as Parkinson's disease and the structure of the inclusion body [30–32]. The origin of amyloid-like aggregate formation in ILs is related to the suppression of protein aggregation. Consequently, we focused on amyloid-like aggregate formation in condensed aqueous solutions of [bmim][NO_3] and [bmim][SCN].

First, we address the case of [bmim][NO_3]. **Figure 7a** shows the FTIR spectra of the eight model proteins, which have different secondary structures and sizes in condensed aqueous [bmim][NO_3] solutions (x = 20). The FTIR spectra of rhodanese, α-chymotrypsin, β-LG, myoglobin, and clearly present peaks at ca. 1615 and ca. 1690 cm^{-1}, are indicating amyloid-like aggregation. In contrast, the four remaining proteins (lysozyme, RNase A, cytochrome c, and insulin) do not present these two peaks. Similar FTIR spectra are also obtained form an aqueous [bmim][Cl] solution at x = 20. To investigate whether the four proteins aggregate, their SAXS profiles were recorded [39]. The SAXS curves show a drastic increase in $I(q)$ below q = 0.03 nm^{-1} for rhodanese, α-chymotrypsin, β-LG, myoglobin, indicating protein aggregation. However, the other four proteins do not aggregate, as indicated by their SAXS

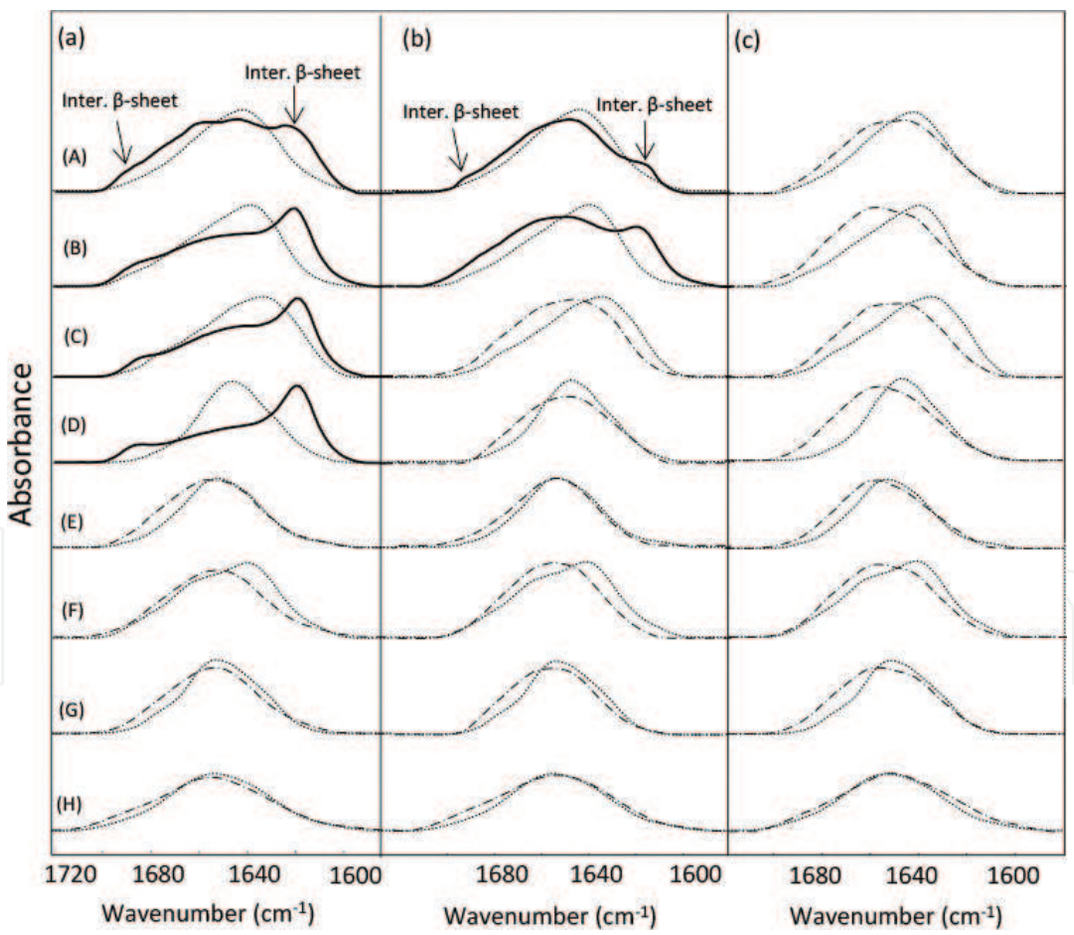

Figure 7. FTIR spectra of various proteins ((A) rhodanese, (B) α-chymotrypsin, (C) β-LG, (D) myoglobin, (E) lysozyme, (F) RNase A, (G) cytochrome c, and (H) insulin) in water (dotted line) and in ILs ((a) [bmim][NO_3], (b) [emim][NO_3], and (c) EAN) solutions (x = 20). The solid and dashed-dotted lines represent aggregated and nonaggregated proteins, respectively.

curves, which do not show a significant increase in $I(q)$ below $q = 0.03$ nm^{-1}. These results are consistent with those from the FTIR experiments. The FTIR and SAXS results indicate that aqueous [bmim][NO_3] solutions at $x = 20$ promote the formation of amyloid-like aggregates in rhodanese, α-chymotrypsin, β-LG, and myoglobin, whereas the same solutions inhibit aggregation for lysozyme, RNase A, cytochrome *c*, and insulin.

Here, to investigate the influence of the imidazolium cation alkyl chain length on the decrease in amyloid-like aggregation, FTIR spectra were recorded for proteins in aqueous solutions ($x = 20$) of [emim][NO_3], which has a shorter alkyl chain length (**Figure 7b**). Intriguingly, the two peaks indicating an intermolecular β-sheet structure are observed for rhodanese and α-chymotrypsin. Conversely, the spectra of the other proteins do not contain these peaks, and the six remaining proteins form an α-helical structure, as in the case of [bmim][NO_3]. The protein size at which aggregation occurs in aqueous [emim][NO_3] solutions is larger than that in aqueous [bmim][NO_3] solutions. Thus, the formation of amyloid-like aggregates depends on the alkyl chain length of the cation.

In order to gain insight into the amyloid-like aggregate formation, we have focused on the solution structure and protein size. As discussed in Section 1, it has been suggested that the structural changes of proteins in aqueous IL solutions are strongly related to the solution structures of these media. 1-Alkyl-3-methylimdazolium-based ILs form nanoheterogeneous structures containing polar and nonpolar domains. The solutions exhibit molten-salt-like behavior, and the water molecules are scattered in the polar domain and self-assemble into confined-water-type domains under IL-rich conditions. The SAXS and small-angle neutron scattering (SANS) results imply that confined water exists in aqueous [bmim][NO_3] solutions at $x = 20$ [18, 19]. Moreover, an increase in alkyl chain length results in an enhancement of nanoheterogeneity [40]. Thus, in the condensed aqueous IL solutions, a decrease in the alkyl chain length of the cation may induce an increase in the size of the confined water domains. In terms of the relationship between the protein structure and the solution structure of the aqueous IL solutions, it has been suggested that proteins in condensed IL solutions are hydrated with water molecules in IL layers [3, 41, 42]. Jaganathan et al. [41] demonstrated the organization of ILs around hydrated cytochrome *c* in high-concentration ILs using molecular dynamics simulations. Similarly, according to the analysis of transfer free energy (ΔG_t) in cyclic dipeptides from water to aqueous IL solutions conducted by Attri and Venkatesu [42], ILs interact unfavorably with protein surfaces, thus promoting the formation of hydration layers around the proteins.

On the basis of these results, we propose that aggregated proteins in aqueous [bmim][NO_3] or [emim][NO_3] solutions at $x = 20$ are even less sufficiently hydrated than the small-sized proteins; therefore, protein-protein interactions are enhanced. However, the nonaggregated proteins selectively interact with water molecules at aggregated water sites in the polar domains. Consequently, the formation of amyloid-like aggregates is strongly related to the size of the confined water domains in the IL layer. Unfortunately, further elucidation of the direct correlation between the protein size and confined water in aqueous IL solutions is difficult. Further experimental studies, such as investigations into the influence of aggregated water in aqueous IL solutions with/without proteins using SAXS and SANS methods, are required.

Next, we discuss amyloid-like aggregation in aqueous [bmim][SCN] solutions showing the strong denaturant. **Figure 8** shows the FTIR spectra of five of the investigated proteins (cytochrome *c*, myoglobin, lysozyme, RNase A, and β-LG) at $x = 30$. Remarkably, the spectra of four of the proteins (with the spectrum of cytochrome *c* being the exception) clearly present peaks attributable to intermolecular β-sheet structures.

To further investigate the changes in the secondary structures of the proteins, we determined their intermolecular-β-sheet contents (β%) using curve-fitting analysis. The β% values at $x = 30$ are 0% for cytochrome *c*, 11 ± 1.6% for myoglobin, 34 ± 3.5% for lysozyme, 21 ± 4.0% for RNase A, and 17 ± 3.2% for β-LG. Compared with the case of [bmim][NO_3], the amyloid-like aggregation patterns do not correlate with the protein size or with their secondary structures. Thus, the origin of the amyloid-like aggregation in aqueous [bmim][SCN] solutions is an interesting topic. When structural transitions of proteins occur in aqueous solutions with salts and ILs, the cations and anions interact directly with specific amino acid residues on the proteins [43, 44], and this interaction is enhanced in condensed IL solutions. Consequently, we focused on the relationship between the secondary-structure content of the proteins in the condensed ILs and their amino acid residue contents.

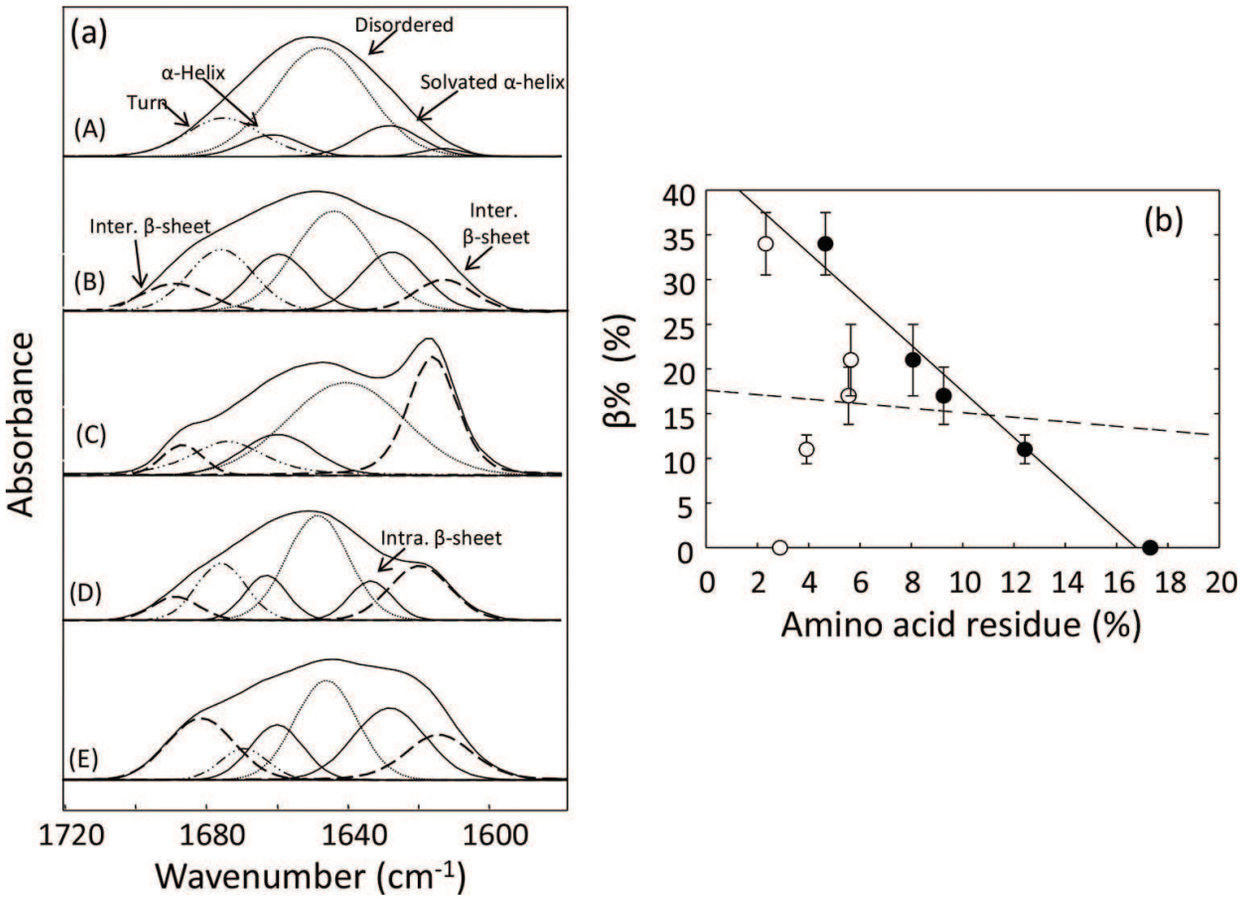

Figure 8. (a) Curve-fitted FTIR spectra in the amide I′ region of (A) cytochrome *c*, (B) myoglobin, (C) lysozyme, (D) RNase A, and (E) β-LG in aqueous [bmim][SCN] solutions at $x = 30$. (b) Relationship between the β% and amino acid residues. Closed and open circles represent Lys and Gln residues, respectively.

To investigate the correlation between the β% values and the occurrence of 20 amino acid residues in the five investigated proteins, we determined the correlation coefficient (R^2) of the relationship between β% and the 20 amino acid residues of the proteins using the slope of **Figure 8b**. **Figure 9a** shows R^2 value between amino acid residues of protein and β%. The value of β% appears to be dependent on the presence of hydrophilic amino acid residues, such as those on Lys, Arg, and Glu residues, rather than on the presence of hydrophobic or aromatic amino acid residues, such as those on Ile, Tyr, and Phe residues. The amino acid residues with $R^2 > 0.7$ are those on Lys, Arg, and Glu residues. Because Lys and Arg residues contain an amino group and Asn and Glu residues contain a carboxyl group, the former tend to interact with SCN^- ions while the latter tend to interact with $[bmim]^+$ ions. An important result is that the Lys residues exhibit the highest R^2 value. A straightforward interpretation of this result is that SCN^- ions bind mainly to the Lys residues of proteins in aqueous solutions. The present result is consistent with the previous X-ray diffraction studies that the SCN^- ions weakly bind to the Lys and Arg residues of proteins in the crystalline state [45, 46].

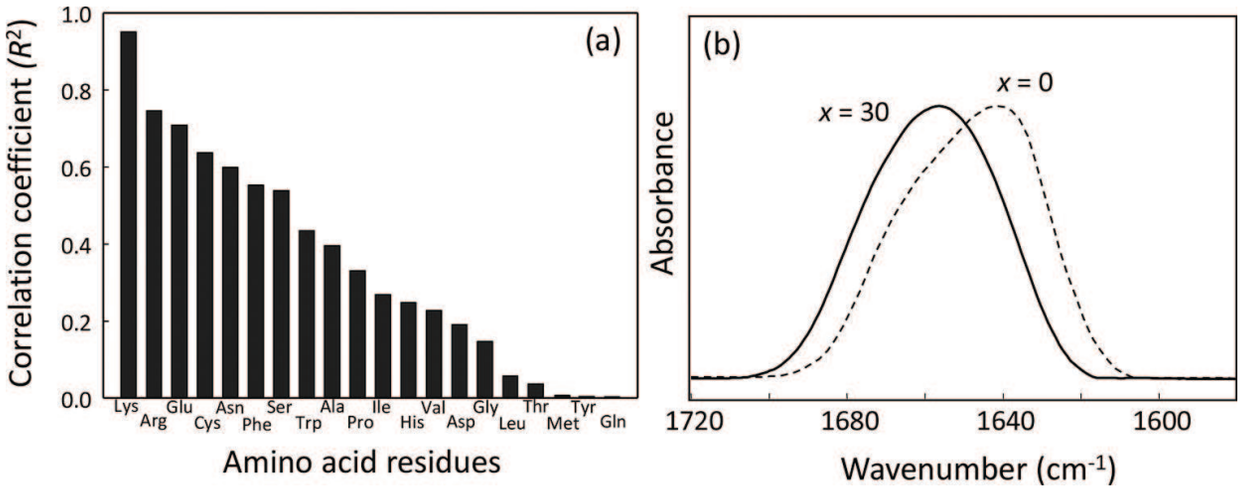

Figure 9. (a) Correlation coefficients (R^2) between amino acid residues of proteins and the content of intermolecular β-sheet structure (β%). (b) FTIR spectra of PLL in aqueous [bmim][SCN] solutions at $x = 0$ and 30.

Here, we can speculate that a Lys-rich polypeptide does not form an intermolecular β-sheet structure in aqueous [bmim][SCN] solutions if Lys residues are directly related to the formation of intermolecular β-sheet structures. To confirm this speculation, we measured the FTIR spectra of poly-L-lysine (PLL) (Lys = 100%) in aqueous [bmim][SCN] solutions at $x = 0$ and 30. They are significantly different from the spectra of the model proteins, in which PLL does not present the two peaks associated with intermolecular β-sheet formation. Accordingly, we propose that the SCN^- ions bind primarily to Lys residues in the proteins, and that Lys-rich proteins do not undergo intermolecular β-sheet formation in the presence of [bmim][SCN]. Thus, the formation of amyloid-like aggregates by the addition of [bmim][SCN] is related to IL-amino acid residue interactions.

These results indicate that the origin of amyloid-like aggregate formation in $[bmim][NO_3]$ is different from that in [bmim][SCN]. The former is due to the relationship between the protein size and the confined water size in the IL layer, while the latter is due to IL-amino acid

residue interactions. The SCN^- anion is a stronger denaturant than the NO_3^- anion. As the denaturation effect of the anions becomes stronger, the origin of amyloid-like aggregation in condensed IL solutions changes from solution structural properties to the IL-amino acid residue interactions.

3.4. Future application of protein engineering

We have discussed the unique structural transitions of proteins in aqueous solutions with [bmim]-based ILs. Aqueous [bmim]-based IL solutions induce two structural transition patterns: the folded state → unfolded state → intermolecular β-sheet aggregation for myoglobin, and the folded state → unfolded state → partial globular state. These transitions are strongly related to solution properties, such as the presence of confined water around the IL layers (i.e., the nanoheterogeneity), a low polarity, and IL-amino acid residue interaction. On the basis of these results, we propose that future applications of ILs in protein engineering may be as cryoprotectants for proteins and as agents for the suppression of amyloid formation.

The inhibition of ice-nucleation and a high structural reversibility of proteins without protein aggregation are important criteria for a protein cryoprotectant. Recently, Yoshimura et al. reported that the aqueous IL solutions in the wide IL concentration range exhibit glassy formation at 77 K [47]. In addition, the present study shows that condensed IL solutions cause the helical formation for some proteins without protein aggregation. Related to these results, we found that low temperatures (77 K) induce structural reversibility for lysozyme in aqueous [bmim][NO_3] solutions [48]. After cooling, the lysozyme structure shows reversible transition without aggregation. Similar results were obtained in the case of RNase A in aqueous solutions of choline dihydrogen phosphate [49]. Thus, condensed IL solutions forming the glassy state at 77 K that induce helical formation without protein aggregation may be applicable as cryoprotectants for proteins, specifically as cryopreservation agents for recombinant proteins. However, in order to use ILs as cryoprotectants, it is necessary to investigate the enzyme activity in condensed IL solutions after cooling and removal of the IL from aqueous protein solutions.

As mentioned in Section 3.3, we have demonstrated that specific IL-amino acid residue interactions in condensed IL solutions cause inhibition of amyloid-like aggregation (i.e., intermolecular β-sheet structures). Related to this, we found that [bmim][SCN], EAN, and PAN ILs suppress thermally induced insulin amyloid formation [50]. Furthermore, condensed solutions of EAN or PAN demonstrate a high protectant ability for the structure of monomeric insulin. The affinity between ILs and specific amino acid residues in insulin is the main cause of the suppression of insulin amyloid formation. Thus, ILs can potentially be used as agents for the suppression of amyloid aggregation.

We proposed the applications of ILs in protein engineering as cryoprotectants for proteins and as agents for the suppression of amyloid formation using properties of the condensed IL solutions. In addition to these, the solution properties of condensed IL solution (the presence of confined water around the IL layers, a low polarity, and IL-amino acid residue interaction) will have a wide potential for applications of ILs in protein engineering in the future.

4. Conclusion

We have investigated the structural transition of proteins in aqueous solutions of ILs over a wide concentration range using FTIR and near-UV CD spectroscopy combined with SAXS. Aqueous IL solutions induced two structural transition patterns; (i) the folded state → unfolded state → partial globular state (α-helical formation disrupted tertiary structure), and (ii) the folded state → unfolded state → aggregation (amyloid-like aggregation or disordered aggregation). These transition patterns are strongly related to the condensed IL solution properties, such as the presence of confined water in the IL layers, low polarity, denaturant effect of anions, and IL-amino acid residue interactions. On the basis of these results, we proposed the new application of ILs as novel cryoprotectants and amyloid suppression agents. The present results will be basic information for the design of ILs for protein engineering applications. Although we have fully investigated the structural properties of proteins in aqueous IL solutions, detailed information on enzyme activity and methods for the removal of ILs from these media is still required to use the protein engineering applications.

Author details

Takahiro Takekiyo* and Yukihiro Yoshimura

*Address all correspondence to: take214@nda.ac.jp

Department of Applied Chemistry, National Defense Academy, Hashirimizu, Yokosuka, Japan

References

[1] van Rantwijk F, Sheldon R A. Biocatalysis in ionic liquids. Chem. Rev. 2007; 107: 2757–2785.

[2] Weingärtner H, Cabrele C, Herrman C. How ionic liquids can help to stabilize native proteins. Phys. Chem. Chem. Phys. 2012; 14: 415–426.

[3] Tietze A A, Bordusa F, Giernoth R, Imhof D, Lenzer T, Mrestani-Klaus C, Neudorf I, Oum K, Reith D, Stark A. On the nature of interactions between ionic liquids and small amino-acid-based biomolecules. ChemPhysChem. 2013; 14: 4044–4064.

[4] Greaves T L, Drummond C J. Protic ionic liquids: evolving structure-property relationship and expanding application. Chem. Rev. 2015; 115: 11379–11448.

[5] Summers C A, Flowers R A. Protein renaturation by the liquid organic salt ethylammonium nitrate. Protein Sci. 2000; 9: 2001–2008.

[6] Lange C, Patil G, Rudolph R. Ionic liquids as refolding additives: N′-alkyl and N′-(ω-hydroxyalkyl) N-methylimidazolium chlorides. Protein Sci. 2005; 14: 2693–2701.

[7] Constantinescu D, Herrman C, Weingärtner H. Pattern of protein unfolding and protein aggregation in ionic liquids. Phys. Chem. Chem. Phys. 2010; 12: 1756–1763.

[8] Constantinescu D, Weingärtner H, Herrman C. Protein denaturation by ionic liquids and the Hofmeister series: a case study of aqueous solutions of ribonuclease A. Angew. Chem. Int. Ed. 2007; 46: 8887–8889.

[9] Zhang Y, Cremer P S. Interaction between macromoleucles and ions: the Hofmeister series. Curr. Opin. Chem. Biol. 2006; 10: 658–663.

[10] Weaver K D, Vrikkis R M, Van Vorst M P, Trullinger J, Vijayaraghavan R, Foureau D M, McKillop I H, MacFarlane D R, Kruger J K, Elliott G D. Structure and function of proteins in hydrated choline dihydrogen phosphate ionic liquid. Phys. Chem. Chem. Phys. 2012; 14: 790–801.

[11] Attei P, Venkatesu P. Ammonium ionic liquids as convenient co-solvents for the structure and stability of succinylated con A. J. Chem. Thermodyn. 2012; 52: 78–88.

[12] Hwang H, Choi H, Kim H –K, Jo D H, Kim T D. Ionic liquids promote amyloid formation from α-synuclein. Anal. Biochem. 2009; 386: 293–295.

[13] Debeljuh N, Barrow C J, Byrne N. The impact of ionic liquids on amyloid fibrilization of Aβ16–22: tuning the rate of fibrilization using a reverse Hofmeister strategy. Phys. Chem. Chem. Phys. 2011; 13: 16534–16536.

[14] Triolo A, Russina O, Bleif H –J, DiCola E. Nanoscale segregation in room temperature ionic liquids. J. Phys. Chem. B. 2006; 111: 4641–4644.

[15] Lopes J N A C, Pádua A A H. Nanostructural organization in ionic liquids. J. Phys. Chem. B. 2006; 110: 3330–3335.

[16] Wang Y, Voth G A. Tail aggregation and domain diffusion in ionic liquids. J. Phys. Chem. B. 2006; 110: 18601–18608.

[17] Jiang W, Wang Y, Voth G A. Molecular dynamics simulation of nanostructural organization in ionic liquid/water mixtures. J. Phys. Chem. B. 2007; 111: 4812–4818.

[18] Abe H, Takekiyo T, Shigemi M, Yoshimura Y, Tsuge S, Hanasaki T, Onishi K, Takata S, Suzuki J. Direct evidence of confined water in room-temperature ionic liquids by complementary use of small-angle X-ray and neutron scattering. J. Phys. Chem. Lett. 2014; 5: 1175–1180.

[19] Abe H, Takekiyo T, Yoshimura Y, Saihara K, Shimizu A. Anomalous freezing of nanoconfined water in room temperature ionic liquid, 1-butyl-3-methylimidazolium nitrate. ChemPhysChem. 2016; 17: 1136–1142.

[20] Smeller L, Meersman F, Heremans K. Refolding studies under pressure: the folding landscape of lysozyme in pressure-temperature plane. Biochim. Biophys. Acta. 2006; 1764: 497–505.

[21] Kelly S M, Jess T J, Price N C. How to study proteins by circular dichroism. Biochim. Biophys. Acta. 2005; 1751: 119–139.

[22] Kozak M. Glucose isomerase from streptomyces rubiginousus—potential molecular weight standard for small-angle x-ray scattering. J. Appl. Cryst. 2005; 38: 555–558.

[23] Hiramatsu H, Kitagawa T. FT-IR approaches on amyloid fibril structure. Biochim. Biophys. Acta. 2006; 1764: 100–107.

[24] Cinelli S, Spinozzi F, Itri R, Finet S, Carsughi F, Onori G, Mariani P. Structural characterization of the pH-denatured states of ferricytochrome-c by synchrotron small angle X-ray scattering. Biophys. J. 2001; 81: 3522–3533.

[25] Takekiyo T, Yamazaki K, Yamaguchi E, Abe H, Yoshimura Y. High ionic liquid concentration-induced structural change of protein in aqueous solution: a case study of lysoyzme. J. Phys. Chem. B. 2012; 116: 11092–11097.

[26] Takekiyo T, Koyama Y, Yamazaki K, Abe H, Yoshimura Y. Ionic liquid-induced formation of α-helical structure of β-lactoglobulin. J. Phys. Chem. B. 2013; 117: 10142–10148.

[27] Takekiyo T, Nihei A, Aono M, Abe H, Yoshimura Y. Optical spectroscopic studies on structural changes of helical-rich proteins in aqueous solutions of ionic liquids. J. Sol. Chem. 2014; 43: 1707–1709.

[28] Takekiyo T, Yamaguchi E, Yoshida K, Kato M, Yamaguchi T, Yoshimura Y. Intercation site between the protein aggregates and thiocyanate ion in aqueous solution: a case study of 1-butyl-3-methylimidazolium thiocyanate. J. Phys. Chem. B. 2015; 119: 6536–6544.

[29] Englasnder S W, Mayne L. The nature of protein folding pathways. Proc. Natl. Acad. Sci. USA. 2014; 111: 15873–15880.

[30] Chiti F, Dobson C M. Protein misfolding, functional amyloids, and human diseases. Annu. Rev. Biochem. 2006; 75: 333–336.

[31] Fink A L. Protein aggregation: folding aggregates, inclusion bodies and amyloid. Fold. Des. 1998; 3: R9–R23.

[32] De Groot N S, Sabate R, Ventura S. Amyloids in bacterial inclusion bodies. Trend. Biochem. Sci. 2009; 34: 408–416.

[33] Shiraki K, Nishikawa K, Goto Y. Trifluoroethanol-induced stabilization of the α-helical structure of β-lactoglobulin: implication for non-hierarchical protein folding. J. Mol. Biol. 1995; 245: 180–194.

[34] Uversky V N, Narizhneva N V, Kirschstein S O, Winter S, Löber G. Conformational transitions provoked by organic solvents in β-lactoglobulin: can a molten globule

like intermediate be induced by the decrease in dielectric constant? Fold. Des. 1997; 2: 163–172.

[35] Hirota N, Mizuno K, Goto Y. Group additive contributions to the alcohol-induced α-helix formation of melittin: implication for the mechanism of the alcohol effects on proteins. J. Mol. Biol. 1998; 275: 365–378.

[36] Wakai C, Oleinikova A, Ott M, Weingärtner H. How polar are ionic liquids? Determination of the static dielectric constant of an imidazolium-based ionic liquid by microwave dielectric spectroscopy. J. Phys. Chem. B. 2005; 109: 17028–17030.

[37] Kindt J T, Schmuttenmaer C A. Far-infrared dielectric properties of polar liquids by femtosecond terahertz pulse spectroscopy. J. Phys. Chem. 1996; 100: 10373–10379.

[38] Chitra R, Smith P E. Properties of 2,2,2-trifluoroethanol and water mixtures. J. Chem. Phys. 2001; 114: 426–435.

[39] Takekiyo T, Fukudome K, Yamazaki K, Abe H, Yoshimura Y. Protein aggregation and partial globular state in aqueous 1-alkyl-3-methylimidazolium nitrate solutions. Chem. Phys. Lett. 2014; 602: 22–27.

[40] Hayes R, Warr G G, Atkin R. Structure and nanostructure in ionic liquids. Chem. Rev. 2015; 115: 6357–6426.

[41] Jaganathan M, Ramakrishanan C, Velmurugan D, Dhathathereyan A. Understanding ethylammonium nitrate stabilized cytochrome c-molecular dynamics and experimental approach. J. Mol. Struct. 2015; 1081:334–341.

[42] Attri P, Venkatesu P. Thermodynamic characterization of the biocompatible ionic liquid effects on protein model compounds and their functional groups. Phys. Chem. Chem. Phys. 2011; 13: 6566–6575.

[43] Shammans S L, Knowles T P J, MacPhee C E, Welland M E, Dobson C M, Devlin G L. Perturbation of the stability of amyloid fibrils through alteration of electrostatic interaction. Biophys. J. 2011; 100: 2783–2791.

[44] Shu Y, Liu M, Chen S, Chen X, Wang J. New insight into molecular interactions of imidazolium ionic liquids with bovine serum albumin. J. Phys. Chem. B. 2011; 115: 12306–12314.

[45] Hamiaux C, Prangé T, Riés-Kautt M, Ducruix A, Lafont S, Astier J P, Veesler S. The decameric structure of bovine pancreatic trypsin inhibitor (BPTI) crystallized from thiocyanate at 2.7Å resolution. Acta Crystallogr. D. 1999; 55: 103–113.

[46] Vaney M C, Broutin I, Retailleau P, Douangamath A, Lafont S, Hamiaux C, Prangé T, Ducruix A, Riès-Kautt M. Structural effects on monovalent anions on polymorphic lysozyme crystals. Acta Crystallogr. D. 2001; 57: 929–940.

[47] Yoshimura Y, Kimura H, Okamoto C, Miyashita T, Imai Y, Abe, Y. Glass transition behavior of ionic liquid, 1-butyl-3-methylimidazolium tetrafluoroborate-H_2O mixed solutions. J. Chem. Thermodyn. 2011; 43: 410–412.

[48] Shigemi M, Mori T, Yamazaki K, Takekiyo T, Abe H, Yoshimura Y. Structural changes of lysozyme in aqueous ionic liquid solution upon heating. Cryobiol. Cryotech. (in Japanese) 2013; 59: 145–148.

[49] Takekiyo T, Yamazaki K, Yoshimura Y. Structural reversibility of protein by the use of a hydrophilic ionic liquid: chloline dihydrogen phosphate. Cryobiol. Cryotech. (in Japanese) 2012; 58: 147–151.

[50] Takekiyo T, Yamaguchi E, Abe H, Yoshimura Y. Suppression effect on the formation of insulin amyloid by the use of ionic liquids. ACS Sustain. Chem. Eng. 2016; 4: 422–428.